JOURNAL OF APPLIED ELECTROCHEMISTRY 6 (1976) 385–396

Electrochemical concentrating and purifying from dilute copper solutions

R. S. WENGER*, D. N. BENNION

Energy and Kinetics Department, School of Engineering and Applied Science, University of California, Los Angeles, California 90024

Received 24 October 1975

The effectiveness of a new process for recovering copper ions from dilute solutions has been tested. Porous, fixed, flow-through graphite electrodes are used in conjunction with a membrane which separates the two feed streams. The concept is demonstrated using a dilute feed of 800 $\mu g\,ml^{-1}$ copper ions which is reduced to less than 1 $\mu g\,ml^{-1}$, and a concentrated stream of 0·4 M copper which is concentrated to 0·7 M. The results show the concept is technically feasible and that it is competitive with existing technology for copper recovery.

1. Introduction

The smelting of copper releases large quantities of SO_2 gas. Increasingly strict pollution laws have prompted developing ways of recovering the SO_2 so it is not released into the atmosphere. An alternative approach is to improve hydro-refining methods which do not release SO_2 gas. It was estimated that by 1970 200 000 tons of copper would be produced by hydrometallurgy (Deco-Trefoil [1]). In hydrometallurgy the copper is dissolved into an aqueous solution in some sort of leaching process. The resulting rich, leach solution is generally too dilute in copper and too concentrated in impurity ions, such as iron, aluminum, and magnesium, to serve as feed to an electrowinning cell. A concentrating and purifying step or steps must usually be located between the leaching and electrowinning steps.

Historically, copper has been precipitated or cemented from dilute solutions using scrap iron. The iron dissolves and the copper precipitates. The resulting copper could be redissolved into concentrated solutions or refined by other means such as smelting. The so-called cement copper is highly impure and the cost of further processing combined with the cost of the iron may be too high compared to that of alternate methods.

Alternative concentrating procedures have been developed which make use of liquid ion exchange resins to remove the ion of interest from dilute leach solutions (Agers *et al.* [2], Agers and De Ment [3]). The resins are selective for specific ions while rejecting to a large extent the impurities. The process takes place in two overall steps. Each overall step contains several separation stages. The first step is absorbing the ion (copper) from dilute leach solutions into the liquid ion exchange resin. The second step is to desorb the copper from the resin into a more concentrated solution of copper ions. A difference in pH between the two solutions is the driving force.

Flow-through, fixed bed type systems might also be used. Several patents were obtained by Carlson [4–6] that deal with ion removal from solutions by electrochemical means. These devices all use porous carbon electrodes with a single feed solution. The metal ions are removed from the solution as it passes through the pores of the electrodes. Work performed by Posey [7] for the removal of copper from distillation plant blowdown utilized a porous cathode packed with fine copper turnings. The unit was designed to remove 90% of the copper present and could be operated virtually without attention.

Recently, Bennion and Newman [8] studied the removal of copper ions from very dilute solutions using porous carbon electrodes as both

* Present address: Spectron Development Laboratories Inc., Costa Mesa, California

anode and cathode. A single feed solution was processed in the cell and the electrodes could be regenerated *in situ* when the cathode became plugged with copper by switching the polarity of the cell. A modified version of the original Bennion and Newman cell is reported on in this paper. The essential difference is the utilization of a membrane separator between anode and cathode compartments to allow two independent feed solutions to be processed.

The present electrochemical device will deplete cations noble to hydrogen in one feed stream while simultaneously concentrating the same ions in another feed stream. Porous, fixed, flow-through graphite bed electrodes are used in conjunction with a membrane to separate the two feed streams. The tests were performed using a dilute feed of approximately 700–800 $\mu g\,ml^{-1}$ in copper and 0·8 M sodium sulphate supporting electrolyte that was reduced to less than 1 $\mu g\,ml^{-1}$ copper, and a concentrated feed of 0·4 M copper sulphate plus 0·8 M sodium sulphate that was enriched to 0·7 M in copper ions.

A primary objective was to determine the maximum throughput of catholyte or dilute feed solution for the given inlet concentration and desired product specification. This was accomplished by determining the limiting current (i.e., the total cell current when the reaction rate is limited by the diffusion of copper ions to the graphite surface) for a number of dilute feed flow rates.

The use of a membrane separator is an important aspect of the design of the device presented here. The membrane, used to separate the anolyte from the catholyte, must be capable of preventing mixing of the feeds due to natural convection while allowing ionic electrical contact between them. Since a certain amount of copper will 'leak' across the membrane from anode to cathode, it is necessary to determine the leakage rate. The effect of this leakage is to reduce the effective cell capacity. Another consideration in choosing a proper membrane separator is its ability to eliminate impurities in the catholyte. The rate of iron ion leakage across the membrane was determined by monitoring the anolyte product for iron over a period of time.

Further testing of the device included the determination of maximum cell operation time before the cathode became plugged with copper deposits or dendritic shorts formed. The shorts formed when copper deposits formed a path between the cathode and the anode. This situation requires that the cell operation be 'switched', that is, polarity and flows are reversed so that the cathode becomes the new anode and vice versa. The cycle period is correlated with cell operating conditions so that it is possible to predict the time between switching.

A summary of the design objectives for the porous electrode model can be made as follows:

High available specific surface area – large mass transfer coefficient.

High driving force for reaction – limiting current.

Long contact time – large ratio of thickness/velocity.

No hydrogen evolution – low potential drop.

High production – high velocity.

High velocity – large electric current.

Large current – high potential drop.

Some of the objectives are conflicting and optimum operating conditions must be predicted.

A number of articles have appeared recently on fixed bed, flow-through electrodes. Alkire and Ng [9] presented a theoretical model for the case where the electrolytic solution flow is perpendicular to the electric current flow. An experimental study on electrodeposition of copper on a single porous bed with parallel solution and electric current flows has been carried out by Chu *et al.* [10]. They present a transient, mass transfer-controlled theoretical analysis of their results. A follow-on article by Chu and Hills [11] considers anodic stripping of the bed and includes surface overpotential control. A recently completed dissertation by Gracon [12] represents a very complete model with surface overpotential effects and comparison to experiment for parallel solution and electric current flow. The anodic oxidation of ferrous iron to ferric iron has been reported on by Adams *et al.* [13].

The work being presented here represents an experimental test of using the anodic stripping and cathodic ion removal operations together for different feed streams using a semipermeable membrane to separate them.

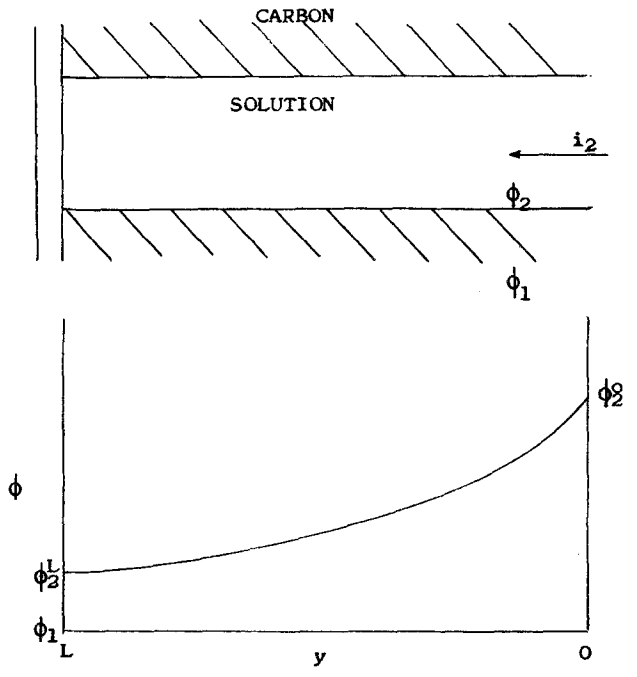

Fig. 1. Potential variation in a pore with electrolytic solution flowing through the pore. $\phi_{2,b}$ is the potential of a hydrogen reference electrode, plus E^0, located along the centreline of the pore. When $\phi^0_{2,b} - \phi_1$ equals E^0, hydrogen evolution occurs at $y = 0$. $\phi^L_{2,b} - \phi_1$ is the total driving force at the rear of the pore and must be large enough to ensure limiting current.

2. Design principles

Theoretical methods for designing the porous cathode include the prediction of the optimum bed thickness and maximum flow rate. This is the maximum thickness and flow rate which will allow reaching limiting current at the back of the electrode while avoiding the evolution of hydrogen at the front. These limits are established by the allowable ohmic potential drop within the porous electrode. The potential difference between the carbon matrix and a reversible copper electrode placed in the bulk solution within the pores formed by the carbon particles (i.e., the surface overpotential plus local concentration overpotential) must be negative enough to ensure that copper is deposited at the limiting current throughout the bed but not so negative as to allow significant evolution of hydrogen.

The mathematical model of the porous, fixed, flow-through electrode system was developed by Bennion and Newman [8]. Six fundamental design equations result. They are as follows:

$$\alpha = \frac{a k_m}{v} \tag{1}$$

$$c_b = c_o e^{-\alpha y} \tag{2}$$

$$i_2 = nFvc_o(e^{-\alpha y} - c_b^L/c_o) \tag{3}$$

$$\phi_{2,b}(y) = \beta(e^{-\alpha y} + \alpha y\, c_b^L/c_o - 1) \tag{4}$$

$$\beta = \frac{nFvc_o}{\alpha\kappa} \tag{5}$$

$$k_m = 0{\cdot}91\ \psi\, v^{0.49}(av\psi)^{0.51}/Sc^{2/3}. \tag{6}$$

From Equation 3 we can obtain an expression for the total cell current recalling that at $y = 0$ all of the current is in the solution phase:

$$i_T = nFvc_o(1 - c_o^L/c_o). \tag{7}$$

A fairly general design constraint for porous electrodes is the maximum allowable ohmic potential drop through the pores. Consider the porous cathode as a single, ideal pore as shown in Fig. 1. A simplified sketch of potential variations from the front, $y = 0$, to the back $y = L$, in the straight tube pore model is shown. The plot of $\phi_{2,b}$ versus y assumes that the conductivity of the electrolyte is small compared to that of the carbon matrix, i.e., ϕ_1 is constant from 0 to L. Values of κ, the electrolyte conductivity, for this application were typically 0·04 mho cm^{-1} for the electrolyte

and 727 mho cm^{-1} for graphite. $\phi_{2,b}$ is the potential in the bulk solution of the pores as measured using a reversible H_2/H^+ reference electrode assuming no pH variation in the pores. Of course, the hydrogen electrode is negative compared to the copper electrode. The curve in Fig. 1 has been shifted up by an amount E°, the difference in rest potential of the hydrogen and copper electrodes in the entrance solution. The driving force for the reduction reaction is $\phi_1 - \phi_{2,s}^y$, i.e., the surface overpotential, where $\phi_{2,s}^y$ is the potential in the solution adjacent to the pore wall just outside the double layer as measured by a reversible Cu/Cu^{++} reference electrode. To process as much feed solution as possible, the driving force must be optimized throughout the bed. The upper limit on $|\phi_1 - \phi_{2,b}|$ is the difference between the equilibrium potentials for the cupric reduction reaction and hydrogen evolution reaction. These quantities are obtained from the Nernst equation and a table of standard electrode potentials. The lower limit on $|\phi_1 - \phi_{2,b}|$ is the minimum potential necessary to ensure limiting current, and is obtained from surface overpotential theory and mass transfer limitations. Hence one can see from Fig. 1 that the optimum bed thickness is that which corresponds to a potential driving force at the front of the electrode, $|\phi_1 - \phi_{2,b}^o|$, just below the allowable maximum and a driving force at the back of the electrode, $|\phi_1 - \phi_{2,b}^L|$, at the allowable minimum.

Further clarification of this concept comes from differentiating Equation 4 with respect to y to obtain:

$$-\frac{d\phi_{2,b}}{dy} = \alpha\beta[\exp(-\alpha y) - c_b^L/c_o] \qquad (8)$$

where

$$\alpha\beta = nFvc_o/\kappa.$$

For a given system, n, F, c_o, and κ will have fixed values and c_b^L/c_o will be specified as the desired product purity. Therefore, the slope of $\phi_{2,b}$ versus y at $y = 0$ will become steeper as the electrolytic solution flow velocity increases, and hence the potential drop in the solution, $\phi_{2,b}^o - \phi_{2,b}^L$, will become larger. The maximum velocity occurs when

$$\phi_{2,b}^o - \phi_{2,b}^L = |\phi_1 - \phi_{2,b}^L|_{min} - |\phi_1 - \phi_{2,b}^o|_{max}. \qquad (9)$$

One can make an order of magnitude estimate of the potential drop through the bed in the solution phase from Equation 4 as

$$\phi_{2,b}^o - \phi_{2,b}^L \doteq \beta = nFv^2c_o/ak_m\kappa. \qquad (10)$$

This equation illustrates the fact that one wants to operate with as high a solution conductivity, κ, as possible. Higher conductivity will allow higher velocities for the potential drop restriction of the system. Equations 1–7 can be solved for the optimum bed thickness, L, and electrolytic solution flow velocity, v, given values for a and $\phi_{2,b}^o - \phi_{2,b}^L$ (Wenger [14]).

A finite plugging time of the cathode is expected since copper is depositing in the interstices of the carbon matrix. If one assumes the cathode is plugged when the void fraction at $y = 0$ is one-half of its initial value, then the time to plugging is determined by dividing the allowable charge passed at the front of the electrode by the rate of charge transfer at $y = 0$. This can be expressed as:

$$t = q_e \Big/ \left(-\frac{di_2}{dy}\Big|_o\right) \qquad (11)$$

where q_e is the amount of charge per unit volume of electrode that must be passed to plate out enough copper so that the void fraction at the electrode front is reduced by one-half. In symbolic terms

$$q_e = nF\rho_{Cu}\epsilon/2M_{Cu} \qquad (12)$$

The quantity di_2/dy is obtained from Equation 3 and is referred to as the transfer current density per unit volume, aj,

$$aj_o = \frac{di_2}{dy}\Big|_o = -nFak_mc_o. \qquad (13)$$

Therefore, the time to plugging of the electrode is expressed as

$$t = \rho_{Cu}\epsilon/2M_{Cu}ak_mc_o. \qquad (14)$$

An important parameter in all of the design equations is the mass transfer coefficient, k_m. The relationship used here is one suggested by Bird *et al.* [15] for Reynolds numbers less than 50 (Equation 6). Other relationships for the mass transfer coefficient are presented by Karabelas *et al.* [16], Mandelbaum and Böhm [17], Williamson *et al.* [18], Wilson and Geankoplis [19], and McCune and Wilhelm [20]. Comparison of all the correlations showed that Equation 6 was

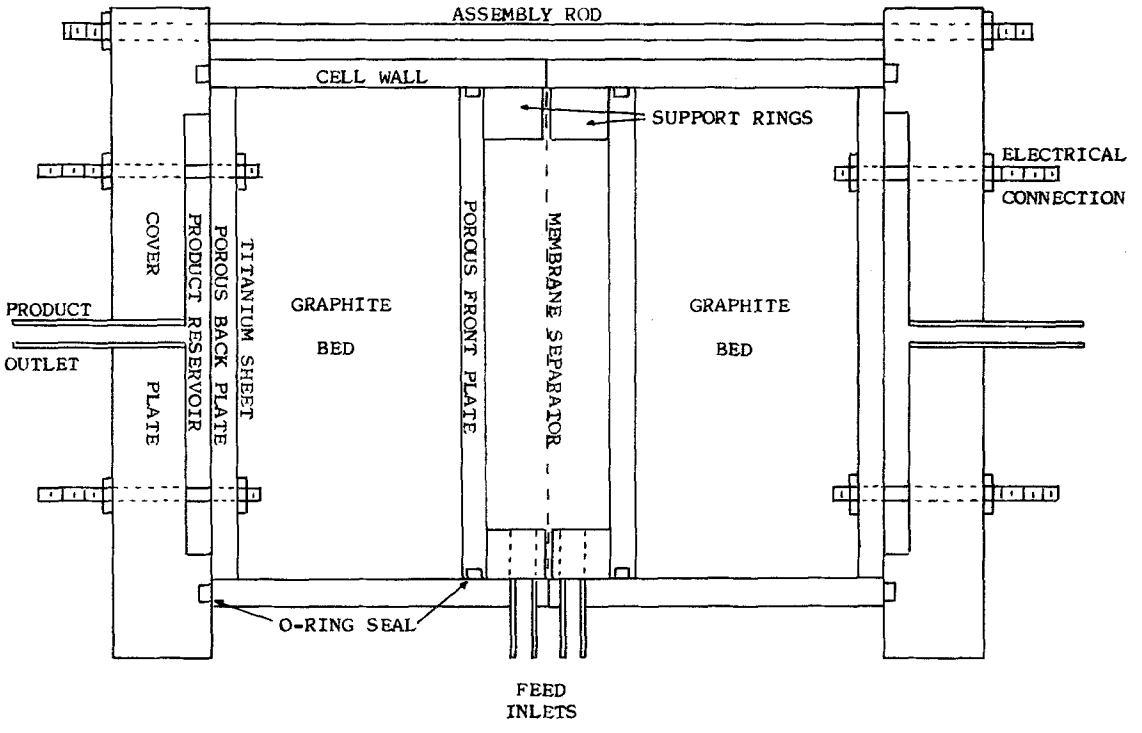

Fig. 2. Experimental cell with 126 cm^2 cross section.

the most conservative, that is, it predicts the lowest k_m, and, hence, it is used in the design calculations.

3. Experimental methods

3.1. *Cell Construction*

The tests were performed on a modified version of the Bennion and Newman design. Overall dimensions of the cell were 12·7 cm in diameter by 20·32 cm long. The cell configuration is shown in Fig. 2. The electrodes consisted of finely divided graphite flakes and chips (Union Carbide GP-22) compressed between two plexiglass plates each drilled with holes to a porosity of 25%. The cell body was made in two halves each constructed of 12·7 cm diameter plexiglass tubing 8·89 cm long. Two cover plates were made from 1·27 cm plexiglass plate cut in a disk shape 17·78 cm in diameter. The cell was assembled using six threaded steel rods that connected the two cover plates. The two halves of the cell were separated with a membrane to prevent mixing of the cathode and anode feeds. Neoprene gaskets were used to seal around the membrane. The gaskets were glued to the edges of the cell body. Electrical connection was made via two stainless steel rods passed through the cover plates and attached to a titanium backing plate. A recess was machined on the inside face of each cover plate to allow a reservoir for product collection.

3.2. *Electrical Equipment*

The power supply for the cell was a Harrison model 6289A DC power supply with both constant current and constant voltage features. Cell voltage was measured with a General Electric DC voltmeter and cell current was measured with a General Electric DC ammeter. Reference electrode potentials were measured with respect to ground with a Keithley model 602 electrometer and recorded on a Sargent model SR strip chart recorder.

The positive lead from the power supply was hooked to the ammeter in series with the cell anode. The negative lead of the power supply and the cell cathode were grounded. Beckman commercial calomel cells placed at various points served as the reference electrodes. The potentials of these cells were used to correlate cell behaviour.

Other system parameters of interest included the pH, temperature, conductivity and concentration of solution at various points in the porous cathode and anode. The solution pH was measured with a Beckman Zeromatic pH meter. Conductivity of electrolytic solution was measured on a Leeds and Northrup model 4959 Conductivity Bridge. Analysis of the solution copper and iron concentrations was performed on a Perkin-Elmer model 303 atomic absorption spectrophotometer. Concentrations above 20 $\mu g\,ml^{-1}$ were diluted with distilled water to the 1–20 $\mu g\,ml^{-1}$ range and then measured after calibrating the instrument with samples of known concentrations.

3.3. *Piping Layout*

Two 60 l primary feed surge tanks contained the dilute and concentrated feeds, and two 20 l head tanks, placed 15 ft above the cell, supplied the solutions to the cell. Continuous circulation between the surge tanks and head tanks was achieved with magnetic drive centrifugal pumps. Two additional tanks were used to collect the products. Feed rates for the cell were controlled on the dilute side with a nuclear products micrometer valve and on the concentrated side with a Hoke 1335G2B valve. Feed rates were measured using a graduated cylinder and stop watch.

3.4. *Procedures*

Reference electrodes were placed at four points in the electrolytic solution streams. One was placed in the dilute product stream, one in the dilute feed stream, one in the concentrated feed stream, and one in the concentrated product stream. The potential of each was measured with respect to the cell cathode and referred to as VDP, VDF, VCF, and VCP, respectively. In this manner it was possible to obtain five separate potential measurements, with respect to ground (the cathode), the fifth being the total cell voltage (VA). To determine the maximum flow rate through the porous cathode, the feed rate to the cathode was set at approximately one-half the predicted maximum rate. Then cell voltage was set at a starting point such that the cell current was about 80% of the expected maximum limiting value. The electrometer lead was connected to the VDP lead and the potential of this calomel cell was recorded on a strip chart recorder. As the cathode product concentration began to fall due to reaction occurring within the pores of the graphite bed, VDP increased. Steady state was assumed after a period of one to two hours when the recorder showed no significant change, less than 0·005 V over a period of 15 min, in VDP. At this point both VDP and cell current were noted and plotted as abscissa and ordinate respectively on linear graph paper. Also, samples of the dilute product and concentrated product were drawn and analysed. Cell voltage, VA, was increased stepwise and the cell was allowed to reach a new steady state. The procedure was continued and the resulting plot of current versus VDP showed a steady increase of current with VDP up to limiting current. Further increases of cell voltage resulted in no significant change in current. However, VDP continued to increase. When cell voltage was increased too far, a second electrode reaction began, hydrogen evolution. Because hydrogen bubbles will tend to plug off part of the electrode, it is desirable to avoid appreciable hydrogen evolution.

It should be noted that VDP plus a constant is a measurement of $(\phi_{2,b}^{L} - \phi_1)$. Some minimum value of VDP must be reached before limiting current (the maximum copper removal rate) is established at the rear of the cathode.

The total current versus VDP curve (see Fig. 3) obtained in this manner for a flow rate below the allowable maximum flow rate will show a flat portion where total cell current will be constant. The plateau begins at a point on the VDP scale where limiting current is first attained and ends at a VDP reading where hydrogen evolution begins. The origin of the plateau was taken at the point where dilute product concentration fell below 1 ppm. The end of the plateau was taken to be at the point where cell current began to rise again.

The next step in determining the maximum flow rate is to increase the dilute feed rate and repeat the above procedure to obtain a new limiting current value. At higher flow rates, the width, on the VDP scale, of the plateau will narrow. At the maximum rate, the plateau will recede to a discontinuity in the slope of the curve. Higher flow rates may be obtained only if the dilute product Cu^{++} concentration is allowed to increase. That is, the feed rate may be increased but not the cell potential.

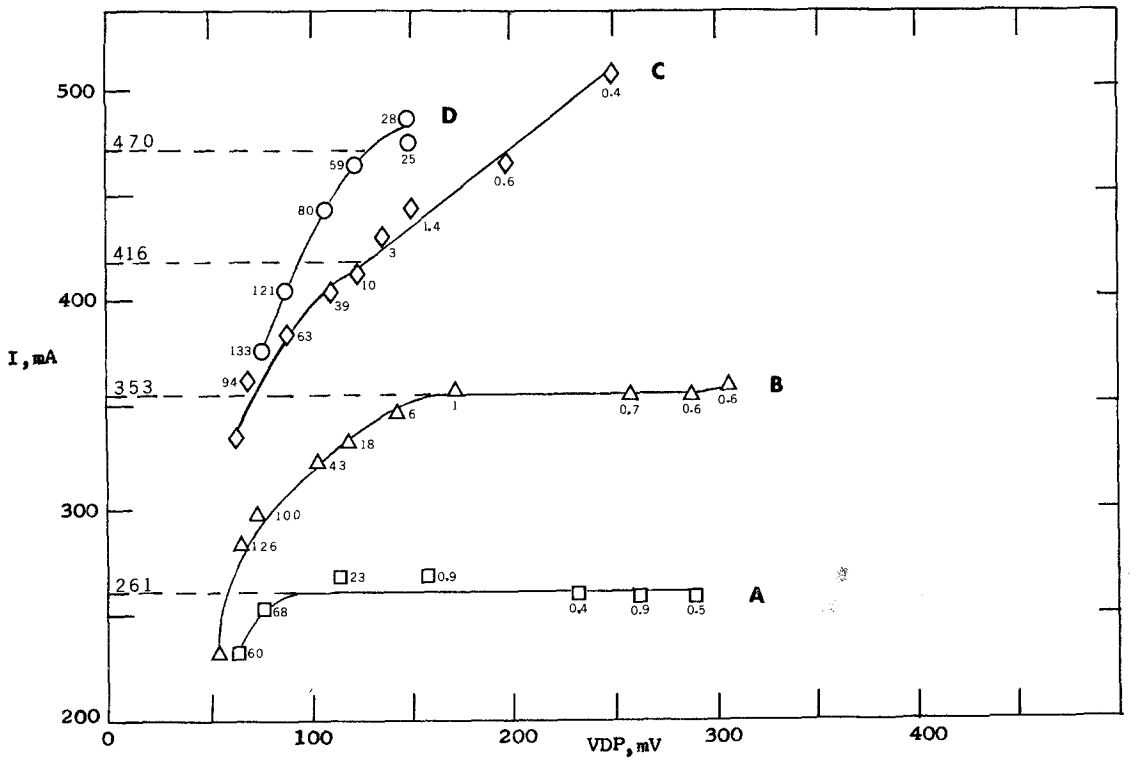

Fig. 3. Limiting current curves. Dashed lines represent calculated limiting currents (see Equation 7). Curve A is for a total flow rate of 6·71 $cm^3\ min^{-1}$; B is 8·60 $cm^3\ min^{-1}$; C is 10·0 $cm^3\ min^{-1}$; D is 12·21 $cm^3\ min^{-1}$.

Plugging time of the cathode was measured during long term runs.

The membrane used in the tests was selected on the basis of its ability to separate anolyte from catholyte by preventing bulk mixing due to ion migration or diffusion. For the latter reasons, primarily migration, an anion exchange membrane seemed to be desirable. Another important requirement for a membrane is its ability to prevent any impurities in the catholyte from entering the anolyte. To test for behaviour in this regard, iron was added to the cathode feed but not to the anode feed. During a long term run, samples of both feeds and products were collected periodically and analysed for iron and copper. Because of iron leakage across the membrane, the anolyte product will increase in iron content.

4. Results

4.1. *Maximum velocity tests*

The limiting current curves for the cell are shown in Fig. 3. Each curve in Fig. 3, A through D, represents a different dilute feed flow rate. Curve A is for a flow rate of 6·71 $cm^3\ min^{-1}$, curve B is for 8·60 $cm^3\ min^{-1}$, curve C is for 10·0 $cm^3\ min^{-1}$, and curve D is for 12·21 $cm^3\ min^{-1}$. The copper concentration in $\mu g\ ml^{-1}$ of the dilute product stream is shown in small numbers adjacent to each datum point. The dashed lines to the left of the curves indicate the calculated value of limiting current for each run (see Equation 7). For this series of tests a total of 26·8 l of dilute solution containing between 780 and 820 $\mu g\ ml^{-1}$ of copper was processed over a period of 48 h. The typical outlet concentration of copper at limiting current was 0·5 $\mu g\ ml^{-1}$. The maximum velocity occurred around 10 or 0·079 $cm^3 min^{-1}$. It can be seen from curve C that the maximum actually lies somewhat below 10 $cm^3 min^{-1}$ since the dilute product concentration is about 10 $\mu g\ ml^{-1}$ at limiting current. The cell potential at the limiting current inflection point of curve C was 1·3 V.

4.2. *Membrane Data*

Impurities in the cathode feed must be excluded

Table 1. Membrane leakage data AMF A-100 membrane A

Date	*Time*	F_A cm/min	C_A^{Cu} μg/ml	C_A^{Fe} μg/ml	F_M μg/min-cm²
7/30/73	3:30P	0·0040	24520	51·6	0·207
7/31/73	8:30A	0·0034	30560	30·2	0·102
8/01/73	8:00A	0·0033	34500	60·0	0·200
8/02/73	8:30A	0·0022	39240	33·5	0·074
	4:30P	0·0022	39240	31·6	0·069
8/03/73	9:00A	0·0027	41320	39·1	0·103
	7:15P	0·0013	42600	49·1	0·065

from the anode product so that a high purity deposit of copper can be obtained in a later electrowinning step. To test the ability of the membrane to prevent contaminants from crossing it and reducing the commercial value of the anode product, iron was added to the catholyte to a concentration of 1150 μg ml^{-1}. The anolyte had an initial iron concentration of 2 μg ml^{-1}. During a long term run, samples of the anode product were collected and the iron level was measured and recorded. The results are shown in Table 1. Generally an increase in the iron concentration of the anode product, C_A^{Fe}, of 40–60 μg Fe ml^{-1} was observed. A representative point on July 30, 1973, at 3·30 p.m. shows an iron level of 51·6 μg ml^{-1} at an anolyte flow velocity, F_A, of 0·004 cm min^{-1}. The iron 'leakage' rate, F_M, is 0·207 μg min^{-1} cm^{-2}. Other leakage rates are shown in the last column. The effluent concentration of copper, C_A^{Cu}, was 24520 μg ml^{-1}, and that for iron was 51·6 μg ml^{-1}. Hence the total copper plus iron concentration was 24572 μg ml^{-1} of which 99·8% is copper.

The leakage rate of copper from the anolyte to catholyte across the membrane was determined to be negligible since good agreement was obtained between the calculated and observed values of limiting current (refer to Fig. 3). If significant copper leakage had occurred, the observed limiting current would have been somewhat higher than the calculated value for a given catholyte flow rate and concentration.

4.3. *Electrode Cycle Life*

Electrode plugging time was measured during another long term run. The results are shown in a plot of cell current versus VDP in Fig. 4. For this run a total of 182 l of dilute feed and 4 l of concentrated feed was processed over a period of 284 h. During this time evaporation and errors in remixing of the feed stock resulted in slight deviations in feed concentration. The horizontal band on the curve represents the range of limiting current. The average cathode product concentration at limiting current was 0·2 μg ml^{-1} and the average anode product concentration was 0·7 M copper. Plugging of the cathode was not observed as such. That is, the cathode flow rate did not decline significantly during the run. However, after running for approximately 12 days at 10·6 cm^3 min^{-1}, a solid path of copper had deposited between the cathode bed through the membrane to the anode bed shorting the cell and preventing proper operation. Hence, an effective cycle life of approximately 10 days seems reasonable with dendrite formation being the limiting factor.

During normal operation, the potential difference between the reference electrode in the cathode feed and the reference electrode in the cathode product, i.e., VDF-VDP, is positive. It was observed that the difference could be allowed to reach around 400 mV before the driving force at $y = 0$ was sufficient to cause hydrogen evolution. Thus, $\phi_{2,b}^{o} - \phi_{2,b}^{L}$ allowable is about 400 mV. Actually the allowable value should be a little less since no correction was made for ohmic losses between the VDF reference electrode and the beginning of the porous electrode. It was noted that after 8 days this potential drop began to decrease. Cell voltage was increased at this point in order to take full advantage of the driving force available, but it was discovered that VDF-VDP continued to decrease. VDP continued to increase as expected, but VDF began to decrease. Approximately 24–30 h before shorting became obvious, the potential difference VDF-VDP passed through

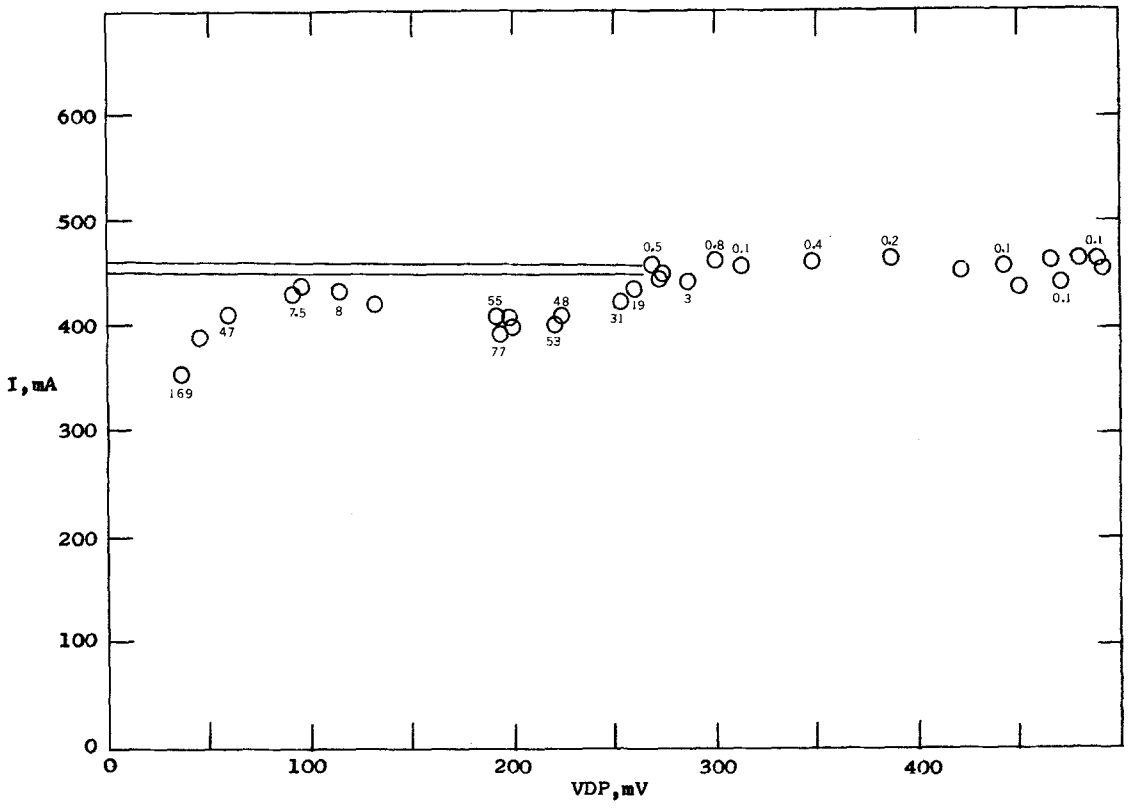

Fig. 4. Limiting current curve during cell plugging tests. Horizontal band represents the variation in predicted values of the limiting current due to evaporation of feed. Small numbers adjacent to data points represent concentration of copper ions in mg ml^{-1}.

zero and became negative. The short became clearly apparent by unsteady behavior, with a significant increase in cell current for a given cell voltage. The decrease in VDP after 8 days was probably due to the first beginnings of dendritic shorting. For a VDP of 114 mV, the total cell potential was 1·14 V. For a VDP of 275 mV, the cell potential was 1·46 V and for a VDP of 348 mV, the cell potential was 1·54 V.

5. Discussion and summary

The limiting current curves shown in Fig. 3 are consistent with what is expected. For a given flow rate the general shape of such a curve should be a steady increase of VDP with cell current, I, up to the limiting current. Then a plateau region is encountered where further increases in cell voltage do not significantly effect the current. When the cell voltage, VA, is sufficiently large so that the combined local concentration plus surface overpotential, $\phi_1 - \phi_{2b}$, at $y = 0$ exceeds the hydrogen evolution potential, cell current will begin to rise again due to the initiation of a second electrode reaction. As long as the hydrogen gas bubbles can be removed smoothly and uniformly, the copper plating reaction will not be affected. However, due to the fact that flow is from front to back in the porous matrix and hydrogen first evolves at the front, the bubbles will be swept deeper into the matrix and at some point will become lodged in a pore. This will tend to plug off part of the reactive surface area and will increase the electrical resistance of the bed. The result will be reduced cell current and increased product copper content. Curve B in Fig. 3 shows very clearly where limiting current and hydrogen evolution begin. The third curve, C, shows the effect of trying to operate in the gassing region. Sufficient time did not elapse to illustrate plugging effects from hydrogen bubbles.

The indicated maximum flow rate from the test results shown in Fig. 3 is 10 cm^3 min^{-1}. This corresponds to a superficial velocity of

0·079 cm min^{-1}. Bennion and Newman [8] observed the maximum velocity to be near 0·2 cm min^{-1}. The theoretical prediction for their system studied is 0·225 cm min^{-1} for a specific surface area of 25 cm^{-1} and an allowed ohmic loss of 0·2 V. For the system studied here the theory predicts 0·199 cm min^{-1} for an a of 24 cm^{-1} and an ohmic loss of 0·205 V. The discrepancy can be attributed to a poor estimate of the specific surface area. Proceeding a step further, for the given result of 0·079 cm min^{-1} maximum velocity, the calculated value of a from the design equations is 18 cm^{-1} and an ohmic drop of 0·08 V. It can be seen that a 25% variation in the value of a affects the velocity prediction by a factor of 2·5. This suggests the importance of predictable, reproducible, and high values of the specific surface area.

For a bed comprised of hexagonal-close-packed spheres, one can derive the relationship for the estimation of a. The graphite flakes ranged in size from 0·1–0·8 mm characteristic dimension. The major portion of the particles were 0·68 mm. Hence one would expect an a of 56·5 cm^{-1}; however, due to the irregular, flake shape of the particles, a large contact area between adjacent particles is probable. This would tend to reduce the exposed reactive surface and reduce a. It is difficult at this point to make an estimate of the percent reduction in useful reactive surface due to irregularly, flake shaped particles. However, a factor of 2 is not unreasonable. Hence, an estimated value of a equal to 25 cm^{-1} is obtained.

The difference between the observed and predicted allowable velocity is probably due to channelling of the flow through the more loosely packed portions of the bed. It appears that an uniformly compressed bed of particles, having a close range of sizes, is desired. Otherwise, the smaller particles will lodge in the interstices of the larger particles and produce irregular flow patterns.

Considering the iron contamination tests, the two nuts used to hold the titanium backing plate in place were type 316 stainless steel. The typical leakage rate observed was 0·207 μg min^{-1} cm^{-2} of iron. The amount of current required to oxidize this amount of iron is 1·33 mA. It is seen that a possible source of the iron contamination was the hold-down nuts. Recognizing this, the anode product contamination rate from iron diffusing across the membrane from catholyte is our upper limit. This suggests that the membrane may be more capable of purification than the data indicate.

Electrode plugging time predicted from Equation 14 is 13 days based on a value of 25 cm^{-1} and $\epsilon = 0{\cdot}5$, operating at limiting current at the maximum allowed velocity observed (10 cm^3 min^{-1}). The cycle was actually terminated due to a dendritic short that formed between the cathode and anode beds. It is possible that membrane materials can be obtained that prevent copper deposits from passing through. Such membranes which prevent zinc dendrites are available for use in zinc silver oxide batteries.

Economic calculations for the proposed system are necessarily dependent upon production rate. For this reason, the maximum velocity through the porous cathode must be predictable. With the establishment of standardized, more optimum procedures for porous electrode construction, the problem of uniform flow should be solved, and thus the expected maximum production rate can be accurately predicted. A reasonable value of the specific surface area is 25 cm^{-1} as discussed above, and the value of $\phi^0_{2,b} - \phi^L_{2,b}$ is 0·2 V. The theoretical maximum velocity for this value of a is 0·22 cm min^{-1}, and the value of L is 5 cm. Based on the corresponding production rate of copper, one can proceed with the economic calculations. An estimate of the cost of materials and construction for a cell 4 ft^2 in cross section has been given by Wenger [14]. This cost is based on actual construction of a 4 ft^2 cell. If one assumes that cell cost increases as the 0·6 power of the scale-up ratio, then the cost of a 32 ft^2 unit will be \$1926·00. The production rate for this single unit at a feed rate of 0·22 cm min^{-1} is 908 060 gal yr^{-1}. A feed containing 0·8 g Cu l^{-1} will yield 6062 lb Cu yr^{-1}. Assuming \$0·10 lb^{-1} commercial value, the gross annual income is \$606·20 yr^{-1}. Total annual cost based on a 5 yr straight line depreciation and 12% return on invested capital is:

Capital cost	\$523·87
Operating labour @ 1/4 MD	20·00
Electrical energy	45·23
Total operating cost	\$589·10 yr^{-1}

The cost per pound of copper recovered is \$0·097 and the cost per thousand gal of feed processed in the porous cathode is \$0·649.

For 1000 such units, the scaled-up installed cost is \$121 522·00 assuming 0·6 power capital cost dependence. The annual cost figures, assuming linear power cost dependence and obtaining labour costs from Peters and Timmerhaus [21], are:

Capital cost	\$ 33 054
Operating labour (19 MH/day)	69 350
Electrical energy	45 230
Total operating cost	\$147 634 yr^{-1}

The total production rate is 908 060 thousand gal yr^{-1}. The amount of copper recovered is 6 061 740 lb yr^{-1} for a total value of \$606 174 yr^{-1} assuming it is worth \$0·10 lb^{-1} in the concentrated solution. The cost per pound of copper recovered is \$0·024 and the cost per thousand gal of feed processed is \$0·163.

6. Conclusion and significance

It is concluded as a result of this work that a copper removal cell capable of removing copper ions from a dilute leach solution and transferring them into a concentrated electrowinning solution is feasible. The membrane is able to adequately separate two independent feed streams, one containing fifty times as much copper as the other, without significant transfer of copper ions across the membrane. Further, it was shown that the cell can be operated in a vertical position, eliminating the need for physical movement of the cell at switching time. These two additional features of the cell over the original design presented by Bennion and Newman [8] make it easily adaptable to many systems requiring concentration and purification of metal ions noble to hydrogen.

Examination of the experimental results indicates that the maximum velocity through the cathode is less than that predicted by the theoretical model based on a bed specific surface area 25 cm^2 cm^{-3}. It is concluded that the non-uniformities in the bed porosity resulted in channelling of the flow and a lower than expected effective surface area of the bed. This channelling reduced the effective exposed surface area such that reduced cell capacity was observed. It is suggested that a more uniform bed packing material be used. Improved packing material should have a high electrical conductivity, be corrosion resistant and provide for uniform flow through the bed.

Acknowledgements

This work was supported by the University of California, Los Angeles, Patent Fund and a grant from the University of California, Los Angeles, Academic Senate.

List of symbols

a	area per unit volume, cm^{-1}
c_o	copper concentration of feed, mol cm^{-3}
c_b	averaged, bulk copper concentration within porous cathode, mol cm^{-3}
c_b^L	copper concentration in cathode effluent, mol cm^{-3}
E^0	potential difference between reversible hydrogen reference electrode and reversible copper reference electrode in solution at y equal zero, V.
F	Faraday's constant, 96 487 coul/equiv
i_2	superficial or overall electrical current density in catholyte solution, A cm^{-2}
i_T	total, overall current density to cathode, A cm^{-2}
j	transfer current density, A cm^{-2}
k_m	mass transfer coefficient, cm s^{-1}
L	thickness of the cathode, cm
M	molecular weight, g $gmol^{-1}$
n	number of electrons transferred in electrode reaction, 2
q_e	charge passed per unit volume of electrode, coul cm^{-3}
Re	Reynolds number, $dv\rho\,\mu^{-1}$
Sc	Schmidt number $\nu\,D^{-1}$, dimensionless
t	time to plug cathode with copper, s
v	superficial or approach velocity of catholyte solution, cm s^{-1}
VDP	potential of saturated calomel reference electrode in catholyte effluent relative to the cathode, V
VA	potential of anode relative to cathode, V
y	distance from entrance of cathode toward cathode backing plate, cm
α	ak_m/v, cm^{-1}
β	$nFv^2c_o/ak_m\kappa$, V
ϵ	void fraction, dimensionless

κ	effective or superficial electrical conductivity of catholyte, mho cm^{-1}
μ	viscosity of feed solution, g $cm^{-1} s^{-1}$
ν	kinematic viscosity, $cm^2 s^{-1}$
ρ	density, g cm^{-3}
ϕ_1	potential in the matrix, V
$\phi_{2,b}$	potential plus a constant of a reversible hydrogen electrode in the solution, V
$\phi_{2,s}$	potential of a reversible copper electrode adjacent to pore wall, V
$\Delta\phi_{ohmic}$	potential difference in bulk solution due to current flow, V
ψ	particle shape factor, 0·86 for flakes, dimensionless

Subscripts

o	front of the electrode
1	solid phase
2	solution phase
b	bulk solution
s	solid–solution interface

References

[1] *Deco Trefoil*, 'Copper-hydrometallurgy', vol. 33, no. 4, Bulletin No. G3-B146 (1969) 9.

[2] D. W. Agers, J. E. House, R. R. Swanson and J. L. Drobnick, 'Copper Recovery from Acid Solutions using Liquid Ion Exchange', General Mills Chemicals, Inc., Minneapolis, Company Report, (not dated).

[3] D. W. Agers, and E. R. DeMent, 'LIX^{R}64 As an Extractant for Copper', Presented at Fall Meeting of the Society for Mining Engineers of AIME, Las Vegas, Nevada, Sept 6–8, 1967, abstract in *Min. Eng.* **19** (1967) 25.

[4] G. A. Carlson, U.S. 3, 459, 646; 5 Aug. 1969.

[5] *Idem*, U.S. 3,647,653; 7 March 1972.

[6] *Idem*, U.S. 3,650,925; 21 March 1972.

[7] F. A. Posey, ORNL-IM-4112, March, 1973.

[8] D. N. Bennion and J. Newman, *J. Appl. Electrochem.* **2** (1972) 113.

[9] R. Alkire and P. K. Ng, *J. Electrochem. Soc.* **121** (1974) 95.

[10] A. K. P. Chu, M. Fleischman and G. J. Hills, *J. Appl. Electrochem.* **4** (1974) 323.

[11] A. K. P. Chu and G. J. Hills, *ibid* **4** (1974) 331.

[12] Gracon, 'Flow Through Porous Electrodes', PhD dissertation, University of Illinois, Urbana (1975).

[13] G. B. Adams, R. P. Hollandsworth and D. N. Bennion, *J. Electrochem. Soc.* **122** (1975) 1043.

[14] R. S. Wenger, 'Electrochemical Concentrating and Purifying from Dilute Copper Solutions', M.S. Thesis, University of California, Los Angeles, Feb. 1974.

[15] R. B. Bird, W. E. Steward and E. N. Lightfoot, 'Transport Phenomena', John Wiley & Sons, New York (1960) pp. 411 and 679.

[16] A. J. Karabelas, T. H. Wegner and T. J. Hanratty, *Chem. Eng. Sci.*, **26** (1971) 1581.

[17] J. A. Mandelbaum, and U. Böhm, *ibid* **28** (1973) 569.

[18] J. E. Williamson, K. E. Bazaire and C. J. Geankoplis *Ind. Eng. Chem.*, **2** (1963) 126.

[19] E. I. Wilson, and C. J. Geankoplis, *ibid* **5** (1966) 9.

[20] L. K. McCune, and R. H. Wilhelm, *ibid* **41** (1949) 1124.

[21] M. S. Peters, and Klaus D. Timmerhaus, 'Plant Design and Economics for Chemical Engineers', 2nd edn., McGraw-Hill (1968) pp. 104 and 131.